Smart Structures and Systems, *Vol. 15, No. 3 (2015) 831-846*
DOI: http://dx.doi.org/10.12989/sss.2015.15.3.831

An innovative hardware emulated simple passive semi-active controller for vibration control of MR dampers

Jianqiu Zhang[1] and Anil K. Agrawal[*2]

[1]*Noise, Vibration and Hardness Expert, HELLA Group, Lippstadt, Germany*
[2]*Department of Civil Engineering, The City College of New York, NY 10031, USA*

(Received November 27, 2014, Revised January 27, 2015, Accepted February 18, 2015)

Abstract. Magneto-Rheological (MR) dampers are being used increasingly because of their adaptability to control algorithms and reliability of passive systems. In this paper, an extensive investigation on performance of MR dampers in semi-active and passive modes has been carried out. It is observed that the overall energy dissipation by MR dampers in passive-on modes is higher than that in semi-active modes for most of the competitive semi-active controllers. Based on the energy dissipation pattern, a novel semi-active controller, termed as "Simple Passive Semi-Active Controller", has been proposed for MR dampers. This controller can be emulated by a simple passive hardware proposed in this paper. The proposed concept of controller "hardware emulation" is innovative and can also be implemented for other semi-active devices for control algorithms of certain form. The effectiveness and reliability of the proposed controller has been investigated extensively through numerical simulations. It has been demonstrated that the proposed controller is competitive to or more effective than other widely used / investigated semi-active controllers.

Keywords: structural response control; passive dampers; semi-active dampers; MR dampers

1. Introduction

Structural control systems, such as passive, semi-active and active control systems, have been investigated extensively during last four decades because of their effective wind and seismic hazard mitigation of civil infrastructures (Spencer and Nagarajaiah 2003). Among the three types of structural control systems, fluid viscous dampers have been used the most extensively in buildings and bridges. For example, 18,338 Taylor fluid viscous dampers have been installed in 484structures for wind and seismic hazard mitigations till 2013 (Taylor Devices 2012).

Significant research efforts have been focused on the semi-active protective systems during the last decade because of their reliability and capability to achieve performance similar to those of fully active systems (He and Agrawal 2006). Semi-active protective systems are able to function as passive devices in the event of failure of the control system or power. These systems are also inherently stable and dissipative, since they cannot input mechanical energy into the structural system. They also require significantly smaller amounts of power compared to an active control system because of parametric nature of the control mechanisms.

*Corresponding author, Professor, E-mail: Agrawal@ccny.cuny.edu

http://www.techno-press.org/?journal=sss&subpage=8 ISSN: 1738-1584 (Print), 1738-1991 (Online)

Among various types of semi-active protective systems, magneto-rheological (MR) dampers have been considered to be particularly promising for both wind and seismic hazard mitigation of structures. MR dampers are similar to conventional fluid dampers in construction. However, they contain MR fluids in place of hydraulic oil in conventional fluid dampers. MR fluids consist of oil with suspended fine iron particles and can change their state from liquid to semi-solid to solid almost instantly in the presence of a magnetic field. Compared to other smart fluids, MR fluids have a large maximum yield stress (50 kpa to 100 kPa), a wide operable temperature range (-50˚C to 150˚C), and a fast response time (milliseconds) (Carlson and Spencer 1996). The performance of MR dampers isn't affected by impurities and contaminants. However, MR dampers are operated in passive-on (PON) mode in majority of applications. In this mode, they are provided with a constant voltage (Chen *et al*. 2003).

Commercial MR fluid devices have been available in the market since middle 1990s (Carlson *et al*. 1996b). However, these devices were considered small scale devices because of force capacity of the scale of 10^3 N. More recently, a large scale 20-ton MR damper was designed and produced by Lord Corporation for full scale seismic applications (Spencer *et al*. 1998a).Mechanical simplicity, high dynamic range, low power requirement, large force capacity and inherent robustness have made large scale MR dampers quite suitable for full-scale structural applications.

A Bouc-Wen model exhibiting hysteretic behavior of the MR damper has been proposed by Spencer *et al*. (1997). Comparison between numerical simulations and experimental results were made to validate the efficiency of this model. The phenomenological Bouc-Wen model was further modified by Jiang *et al*. (2010) to better accommodate a time varying current. More recently, a hyperbolic tangent model has been presented by Bass *et al*. (2007) to model the behavior of MR dampers. This model describes the dynamics of the damper and the force output in a state space form, making this model suitable for a faster numerical analysis (Jiang *et al*. 2010).

Although numerous semi-active control algorithms have been proposed in the literature, it has been observed that the performances of MR dampers using currently available semi-active controllers are inferior to or is similar to those of MR dampers in PON modes. For example, Friedman *et al*. (2014) have carried out a detailed investigation on the performance of PON and COC controllers and have shown that the performance of PON is better or similar to COC. In this paper, the performances of two most competitive semi-active controllers for MR dampers have been compared with those of MR dampers in PON mode. Based on this investigation, a "Simple Passive Semi-Active Controller" (SPSAC) has been developed. Although this is semi-active controller, it can be implemented as a passive system (i.e., without requiring sensor and controller).

2. Performance of MR dampers in semi-active and PON modes

An extensive comparative investigation on performances of MR dampers in semi-active and PON modes have been carried out through numerical simulations on a 4-story evaluation model representing the moment resisting frame of a typical office building on stiff soil in Los Angeles, California. Detailed information on the property of this building and the development of the evaluation model can be found in Friedman *et al*. (2010). Fig. 1 shows the 13 degrees of freedom evaluation model consisting of eight horizontal DOFs and five vertical DOF (Zhang 2012). The first five natural frequencies for the structural model are 0.70, 1.82, 3.36, 5.22, 5.36 Hz.

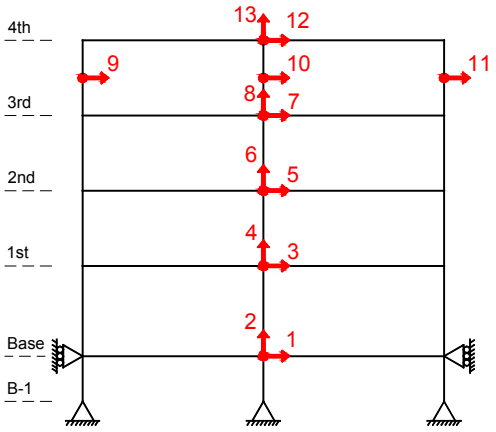

Fig. 1 Evaluation Model of the Moment Resisting Frame for Numerical Simulation

The model of MR damper in the numerical simulations is based on a 200 kN MR damper with a stroke of 584 mm. The phenomenological Bouc-Wen model for MR dampers discussed previously requires ten parameters as a function of current in the damper to fully characterize the dynamic behavior of the MR dampers. Polynomial functions for these parameters as a function of the current i are have been obtained by nonlinear optimization of model parameters using experimental data of MR dampers (Zhang 2012). Likewise, fourth order polynomial functions for parameters of the hyperbolic tangent model as functions of the current (i) have been derived by Jiang *et al*. (2010) through optimization using experimental data on MR dampers. Results by Jiang *et al*. (2010) show that, although both the Bouc-Wen and the hyperbolic-tangent models can predict the control force of the 200 kN MR damper very well, RMS errors (between experimental and theoretical responses related to dampers) are smaller in case of the hyperbolic-tangent model. They have shown that the hyperbolic-tangent model is 20% faster than the Bouc-Wen model. In this research, both Buoc-Wen and hyperbolic-tangent models has been used to model behavior of MR dampers.

The performance of large scale MR dampers in semi-active and passive-on modes has been evaluated by selecting two very competitive and widely investigated semi-active controllers: (i) Clipped-Optimal Controller (COC) (Jansen and Dyke 2000) and smooth boundary layer controller (SBLC) (He *et al*. 2003). The COC consists of two sub-controllers: a linear optimal controller and a secondary bang-bang controller. The force calculated by the linear optimal controller (the first sub-controller) can be generally expressed as

$$f_c = L^{-1}\left\{K_c(s)L\{\begin{bmatrix} y \\ f \end{bmatrix}\}\right\} \tag{1}$$

where y is the vector of measured structural response; f is the vector of measured force generated between MR dampers and the structure; $L\{\cdot\}$ and $L^{-1}\{\cdot\}$are the Laplace transform and inverse Laplace transforms, respectively; and $K_c(s)$ is a linear optimal controller designed to provide the desired control force based on the measured responses y and the measured force f. The term f_c is the optimal control force calculated by the linear optimal controller (or the first sub-controller of COC). It is noted that the linear optimal controller $K_c(s)$ can be obtained from a

variety of synthesis methods, e.g., LQG. In the COC, the rule based on which the control voltage is generated is stated as: (1) when the MR damper is providing the desired optimal force (i.e., $f = f_c$), the voltage applied to the damper should remain at the present level; (2) if the magnitude of the force produced by the damper is smaller than the magnitude of the desired optimal force, and the two forces have the same sign, the voltage applied to the current driver is increased to the maximum level so as to increase the force produced by the damper match the desired control force; (3) otherwise, the voltage applied to the current driver is set to zero. The algorithm for selecting the command signal can be expressed as

$$v = V_{max} H\{(f_c - f)f\} \tag{2}$$

where V_{max} is the voltage to the current driver associated with saturation of the magnetic field in the MR damper, and $H\{\cdot\}$ is the Heaviside step function.

The smooth boundary layer controller (SBLC) was developed by He *et al*. (2003) and has been modified for MR dampers as

$$u(t) = \beta \left| P\left[\dot{d}(t)\right] \right| tanh(\alpha d) \tag{3}$$

where u is the control voltage; term d is the displacement across the damper; α and β are the weighting parameters to be defined by the designers;$\left| P\left[\dot{d}(t)\right] \right|$is the absolute value of the local peak displacement prior to the current time t. According to the control algorithm, the control voltage is determined by the velocity across the damper through a hyperbolic-tangent function. The hyperbolic-tangent function ensures that the control voltage will decrease to zero smoothly (the design parameter α controls how smooth this voltage-drop is) when the damper stops moving.Performance of this controller has been investigated extensively by He *et al*. (2003).

Nine evaluation criteria, similar to those used in several benchmark studies (Ohtori *et al*. 1998b, Agrawal *et al*. 2009), have been used to evaluate performance of MR dampers in semi-active and PON modes. However, among these 9 evaluation criteria, evaluation criteria J_1, J_2 and J_6 shown in Table 1 have been considered to be more important measures. The importance of these criteria lies in their definitions: J_1 (normalized displacement) and J_2 (normalized interstory drift) are related to the maximum damage caused to the structure, while J_6(normalized norm of drift) is related to cumulative seismic damage during the duration (t_f) of the earthquake. In these evaluation criteria, $x_i(t)$ is the horizontal displacement of i^{th} floor; x_{max} is the maximum displacement of the uncontrolled structure for a particular earthquake;$d_i(t)$ is the inter-story drift of the ith floor; h_i is the height of ith floor and$d_{n,max} = \max(d_i(t)/h_i)$ is the uncontrolled maximum inter-story drift ratio. Evaluation criteria J_6 corresponds to normed response quantities (e.g.,$\|x_i(t)\| = \sqrt{\int_0^{t_f} x_i^2(t)dt}$).

Four recorded earthquakes, which have also been adopted in several benchmark structural control studies (Agrawal *et al*. 2009), have been selected for this study. These four historical ground motions are: (1) El Centro (N-S, 1940), (2) Hachinohe (N-S, 1968), (3) Kobe (N-S, 1995), (4) Northridge (N-S at Sylmar County Hospital parking lot, 1994). These earthquakes are denoted as ELC, HAC, KOB and NOR, respectively.

Two 200 kN MR dampers, one between Base and 1stfloor and another between 1st and 2nd floor, have been installed in the evaluation model in Fig. 1. As described previously, COC consists of two sub-controllers: a linear optimal controller in Eq. (1) and a secondary bang-bang controller in Eq. (2). A state-space linear quadratic Gaussian (LQG) regulator is chosen as the linear optimal

controller to calculate the optimal control force. The LQG controller has been designed by considering floor accelerations as measured responses, weighting matrix$Q = q[I]$) and control weighting matrix R = a $[4 \times 4]$ diagonal matrix with R(1,1) = R(2,2)= r, and R(3,3)= R(4,4) = 0 (Zhang 2012).Parameters for COC and SBLC controllers have been designed using El Centro earthquake such that (1) the normalized inter-story drift (J_2) is minimized, and (2) the force capacity (200 kN) of MR damper is fully utilized. Resulting design parameters of above two controllers are: $q = 1 \times 10^{10}$, $r = 1 \times 10^{-5}$ for COC, $\alpha = 20$, $\beta = 40$ for SBLC. In addition, a saturation voltage V_{max} = 2.5 volt is designated for all the controllers to avoid damage to MR damper coils. It should be noted that weighting matrices Q and R are the weights on the response reduction and control cost in a typical LQG controller (Friedman *et al*. 2014).

Simulation results have been analyzed for 4 earthquakes described previously. It has been observed from simulation results that while passive-off case is almost similar to the uncontrolled case, performances of other three controllers are quite similar. In fact, the performance of PON controller is better than two semi-active controllers during Northridge earthquake, which is the most severe among 4 earthquakes, although other earthquakes also yield similar results (Zhang 2012).

It has been observed from simulation results that the maximum peak control force during passive-off case is around 0.5% of the effective seismic weight. During semi-active modes, the peak control force is increased to 2% of the effective seismic weight, since there are two MR dampers of 200 kN capacity each. Hence the reduction of peak response quantities in semi-active case is more obvious as compared to the passive-off case. Such reduction in the structural responses can be further quantified by calculating the evaluation term "Gain/Loss of J", which is percentage response reduction. The Gain/Loss of J (shortened as GLJ) for a controller with respect to uncontrolled response can be calculated as

$$GLJ^{COC,EQ}_{Uncontrolled,i} = \left(1 - J_i^{COC,EQ}\right) \times 100\%; \quad GLJ^{SBLC,EQ}_{Uncontrolled,i} = \left(1 - J_i^{SBLC,EQ}\right) \times 100\% \quad (4)$$

where subscript i denotes evaluation criteria number, the label EQ (= ELC, HAC, KOB, NOR) is the ground motion under which the criteria J_i has been obtained. The calculated GLJ error directly reflects gain or loss in the performance of a specific control strategy with respect to uncontrolled response. When a control strategy fails to reduce the structural responses, the sign of the calculated error would be negative; and the magnitude of the absolute value of this negative error represents increase in response with respect to uncontrolled structure.

Table 1 Evaluation Criteria for the Performance Comparison

Peak Horizontal Disp.	Peak Interstory Disp.	Normed Interstory Disp.
$J_1 = max\left(\frac{max\lvert x_i(t)\rvert}{x_{max}}\right)$	$J_2 = max(\frac{max\lvert d_i(t)/h_i\rvert}{d_{n,max}})$	$J_6 = max(\frac{max\frac{\lVert x_i(t)\rVert}{h_i}}{\lVert d^{max}\rVert})$ Peak Absolute

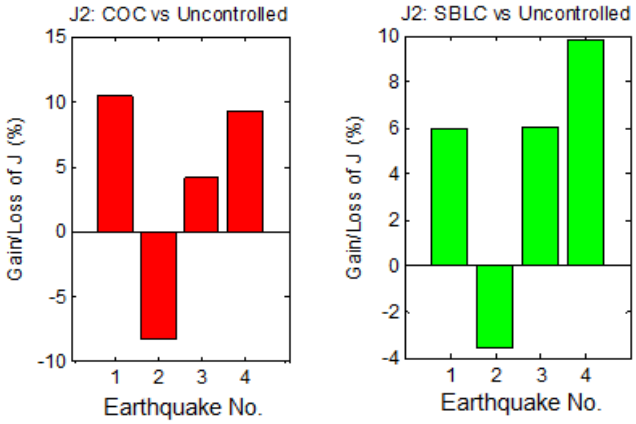

Fig. 2 Plots of Gain/Loss of J2for COC SBLC with Respect to Uncontrolled Responses

It has been observed from simulation results that the evaluation criteria $J_6$is generally more than 15% in cases of both COC and SBLC for all earthquakes and J_1 is positive for both controllers during all 4 earthquakes, although it is close to zero for COC during Hachinohe earthquake. In particular, the SBLC reduces the cumulative floor displacement (J_6) by more than 20% during Hachinohe, Kobe, and Northridge earthquakes, and 32% during the El Centro earthquake. Hence, bar plots only for the evaluation criteria J2 (interstory drift) are shown for two controllers in the Fig. 3 below. Evaluation criteria J_2 for the Hachinohe earthquake (earthquake 2) shows a loss in Fig. 3, whereas J_6 for this earthquake has been found to be a gain for both COC and SBLC controllers. This shows that the two controllers are more effective in reducing the overall interstory drift time-history of the building and not effective in reducing the peak interstory drift during the Hachinohe earthquake. However, overall the SBLC is more effective in reducing the peak drift than the COC.

Although the two semi-active controllers achieved a better performance than the passive-off mode, both controllers have been observed to achieve a performance similar to that of the passive-on mode (Zhang 2012). To better illustrate of the two controllers with respect to the PON case, a quantified comparison is made by calculating the GLJ for COC and SBLC cases with respect to PON during the four earthquakes. The GLJ is calculated with respect to passive-on case using the following equations,

$$GLJ_{PON,i}^{COC,EQ} = \left(J_i^{PON,EQ} - J_i^{COC,EQ}\right) \times 100\%; \; GLJ_{PON,i}^{SBLC,EQ} = \left(J_i^{PON,EQ} - J_i^{SBLC,EQ}\right) \times 100\% \quad (5)$$

where i represents subscript for evaluation criteria J_i, and label EQ (= ELC, HAC, KOB, NOR) indicates the ground motion. A positive GLJ calculated by Eq. (5) indicates that MR dampers in semi-active mode achieves a better performance than the passive-on case, while a negative GLJ implies an inferior performance of MR dampers in semi-active mode with respect to the passive-on case. Fig. 4 shows GLJ for COC and SBLC with respect to the PON case.

Out of the total twelve $GLJ_{PON,i}^{COC,EQ}$ shown in Fig. 5 for the COC case, only three values ($GLJ_{PON,1}^{COC,ELC}$, $GLJ_{PON,1}^{COC,HAC}$, $GLJ_{PON,2}^{COC,HAC}$) are found to be positive. On the other hand, 5 $GLJ_{PON,i}^{SBLC,EQ}$ values are positive for the SBLC case. In particular, among 8 GLJ values for the evaluation

criterion J_6 for COC and SBLC, only $GLJ_{PON,6}^{COC,KOB}$ shows an improvement of 1% over the PON case. Considering the fact that semi-active controllers utilize advanced control algorithms and sensors for achieving an optimized control of structural responses, their performance in Fig. 5 is not attractive for practical applications.

3. Energy dissipation pattern

The performance of the damper as well as the controller largely depends on the amount of the dissipated seismic energy and the way in which the energy is dissipated during the earthquake ground motion. The energy dissipation by the 200 kN MR damper occurs during each of the reciprocating piston strokes as the structure is subjected to external load. The total energy dissipated (E_D) by a MR damper during a displacement interval of $[x_1, x_2]$ can be calculated as (Chopra 2001)

$$E_D = \int f_D \cdot d(x_d) \,, \qquad x_d \in [x_1, x_2] \tag{6}$$

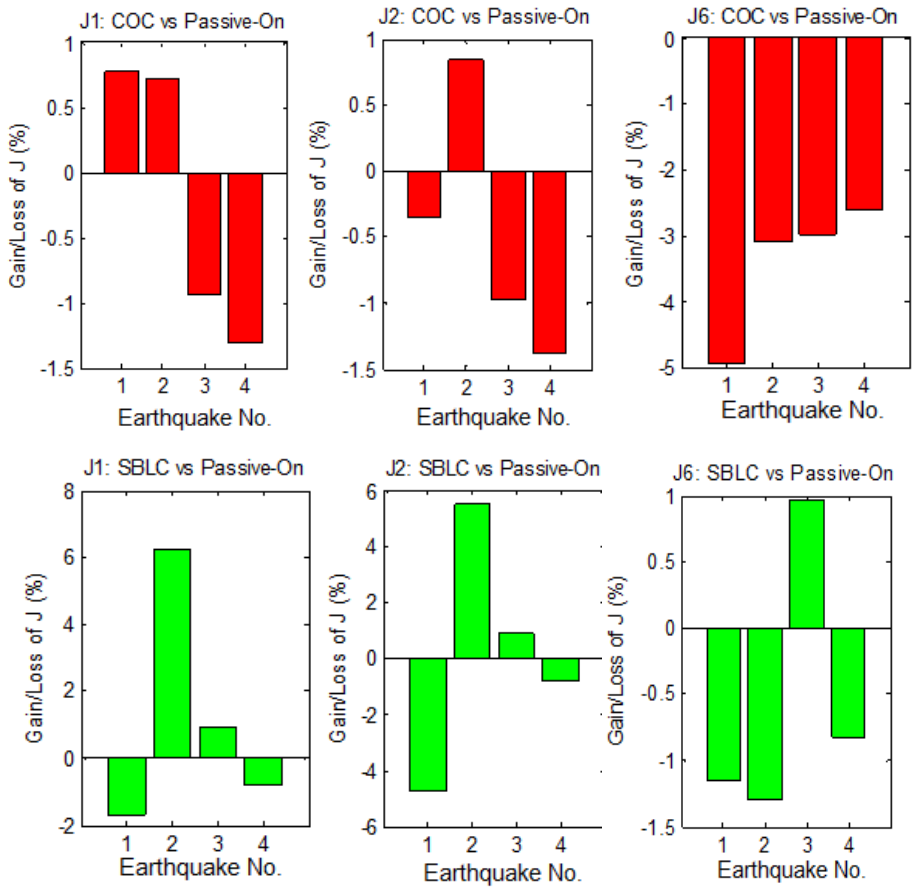

Fig. 3 Plots of Gain/Loss of J between COC and Passive-On Cases

In Eq. (6), f_D is the damper force, x_d is the damper piston movement (equivalent to inter-story displacement when damper is horizontally connected between two stories), x_1 and x_2 are the lower and upper limits of the displacement interval of interest.

In order to investigate energy dissipation pattern of MR dampers in semi-active and passive modes, numerical simulations have been carried out by installing two MR dampers in the building (one in base floor and one in 1st floor in Fig. 1) subjected to the El Centro earthquake. Both MR dampers have been controlled in passive-on (Constant voltages of 2.0 V for damper 1 on first floor and 1.0 V for damper 2 on second floor) and semi-active control (COC) modes. Energy dissipated by MR dampers has been calculated from numerical simulation results using Eq. (8).

Fig. 6 shows the plots of energy dissipated by the MR Damper 1 as a function of inter-story drift (or damper stroke) for the two control strategies (COC and passive-on). The bars in the figure represent the amount of cumulative dissipated energy within each damper stroke interval. The plots for MR Damper 2 and those during other earthquakes have been found to be similar to those in Fig. 6.

It is observed from Fig. 6 that the pattern of the dissipated energy distribution is nearly triangular, and most of the energy is dissipated around the zero interstory drift (or maximum interstory velocity during each vibration cycle). For example, total energy dissipated by MR Damper 1 in PON mode is 268.6 kN·m, the maximum interstory drift of that floor is 0.035 m, and 68% (183.1 kN·m) of the total dissipated energy occurs within ±0.01 m displacement around the zero position of the piston. For the case of COC in Figure 6, 64% (110.7 kN·m) of the total energy is dissipated within ±0.01 m displacement around the zero position of the piston. It is interesting to note that, although clipped-optimal controller utilizes sophisticated sensor-based feedback control logic, its dissipated energy distribution is very similar to that of the PON case. It has been observed from simulation results that the total energy dissipated by MR damper 1 in PON mode (268.6 kN·m) is 55% more than the amount dissipated (173.0 kN·m) in COC mode. Such significant difference in dissipated energy can explain why the performance of MR dampers in semi-active model is inferior to that in PON mode.

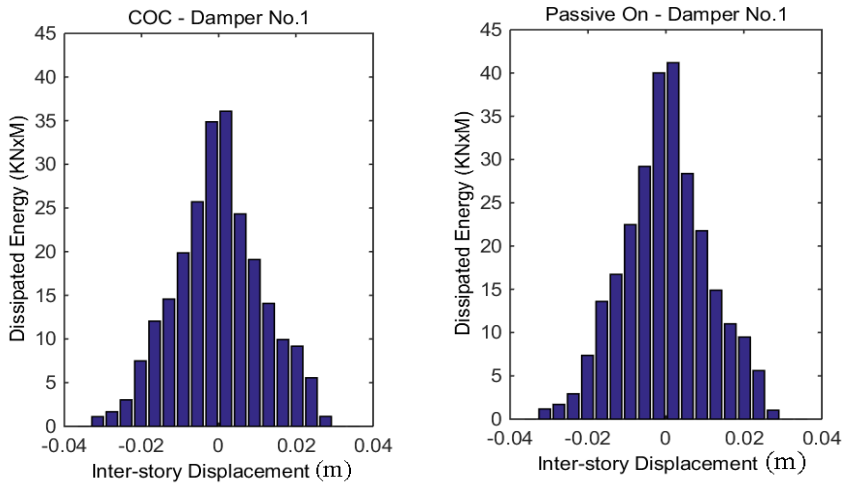

Fig. 6 Energy Dissipation Pattern by MR Damper in Semi-active and PON Modes

4. Development of an innovative simple passive controller

It has been observed from results presented above that the dissipated energy (E_D) is a function of the control force (f_D) and the damper piston displacement (x_D). For MR dampers, the magnitude of control force f_D is determined by the control voltage and the damper piston movement. Fig. 7 shows the force-displacement and force-velocity relationships obtained during the MR damper characterization testing. Green (light black in print paper) and black loops are the force-displacement loops of the 200 kN MR damper obtained using different testing facilities. Each loop in Fig. 7(a) is the force-displacement relationship under a different constant current. It is observed that when the control current increases from 0 A to 2.5 A, the magnitude of the peak damper force jumps from a minimum of ±15 kN to a maximum of ±200 kN. Maximum values of damper forces in both stroke directions in each loop are around x_D= 0 mm. It is also observed from Fig. 7(a) that the damper force drops to zero at the maximum strokes of ±25 mm. Essentially, the velocity is the maximum at zero stroke and decreases gradually as the stroke increases to its maximum value. Hence, no control force can be generated at the instant of the maximum stroke. It is observed from the force velocity loop in Fig. 7(b) that the peak value of damper force increases with an increase in the control current or voltage and maximum force appears at tip-ends of each "S" shape hysteretic loop. The full force capacity (200 kN) of the damper is utilized when both the voltage and the velocity reach their peak values.

Hence, a regulation of the control force magnitude cannot be achieved by merely changing the control voltage when the piston movement is slow. Likewise, decreasing the voltage at the moment when the piston velocity is large is not an "optimal" control option because larger amount of seismic energy could be dissipated if the voltage is kept high at the instant of high velocity. Based on these observations, a concept of simple-passive semi-active controller (SPSAC) is proposed as: input a high voltage to the MR damper to generate a relatively large control force when the floor with dampers or the damper piston vibrates across its zero position. Both the high input voltage and large input velocity will guarantee a large output force and lead to maximum energy dissipation. However, keeping the MR damper working under high voltage (e.g., 2.5 volt) for a long duration may result in a floor lock-up, thus increasing the absolute acceleration of the floors with dampers and drifts of floors without dampers (Jansen *et al*. 2000). The proposed SP controller to maximize the energy dissipation as well as to avoid the floor lock-up is described as

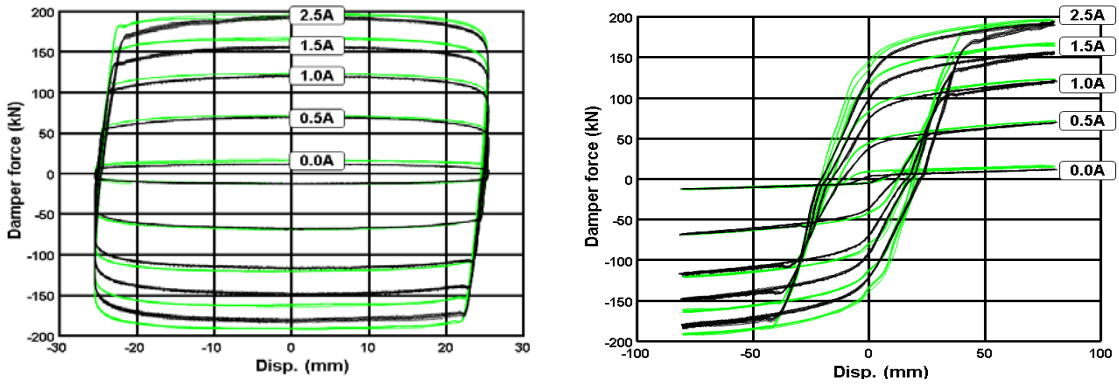

Fig. 7 Behavior of MR Dampers: (a) Force-Displacement Loops and (b) Force Velocity Loops

$$V=\begin{cases} V_1 & |X|<X_1 \\ V_2 & X_1\le|X|<X_1+X_2 \\ V_3 & X_1+X_2\le|X|<X_1+X_2+X_3 \\ 0 & X_1+X_2+X_3\le|X| \end{cases} \tag{7}$$

where V is the control voltage; X (in m) is the damper piston movement or inter-story displacement of the floor on which the MR damper is horizontally installed;X_1, X_2,X_3 ,V_1, V_2, and $V_3$are the design parameters to be determined based on control objectives. The proposed SP control algorithm is represented graphically in Fig. 8 below.

According to the SPSAC algorithm in Eq. (7) and Fig. 8, a voltage of V_1will be input to the damper when the piston displacement or the inter-story drift is within the range of $\pm X_1$. When the floor swings away from its undeformed position beyondX_1, the control voltage drops to V_2 in order to avoid locking up of the floor. However, as the peak inter-story drift increases, voltage will be increased to V_3 after the threshold drift X_1+X_2 so that the damper can act as a stiffness element to limit the peak inter-story drift. Note that the voltage is dropped from V_3 to zero for $|X|\ge X_1+X_2+X_3$, since the relatively high voltage V_3 can only be allowed to last for a short time period (usually 1 to 2 seconds) in order to avoid any permanent damage to the wired-coil in the piston. It should be noted that the controller parameters X_1, X_2, X_3 , V_1, V_2, and V_3 can be identified through a multi-objective optimization for a particular structure subject to selected ground motions.

5. Emulation of SP controller using mechanical-electrical devices

All semi-active controllers require computational equipment (e.g., embedded microcontroller) inevitable for practical implementation of semi-active controllers. One of the innovative aspects of the proposed SPSAC is its emulation using mechatronics components, thereby eliminating the need for sensors, signal filters, computers/microcontrollers. This will not only enhance system stability and reliability, but will also make practical applications easier. Reliability of a semi-control system in a harsh environment is the biggest impediment in its implementation.

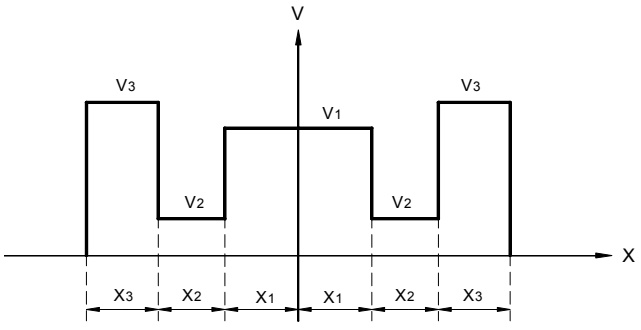

Fig. 8 Voltage Displacement Plot of Proposed Simple Passive Semi-Active Controller

The emulation of the SPSAC can be realized using a concept device called "electrical plate". Considering the control logic in Fig. 8 with voltages (V_1,V_2, and V_3) and linear section lengths (X_1, X_2 and X_3), an electrical plate can be manufactured as illustrated in Fig. 9. Essentially, the electrical plate consists of short metal pieces of lengths X_1, X_2 and X_3. Each of these metal pieces is supplied with voltagesV_1, V_2 or V_3 as per the logic in Fig. 9. Using a common battery power, all the metal pieces can be supplied by a desired voltage V_i for a length of X_i using a simple electrical circuit illustrated in Fig. 9. The operational voltage for most of the MR dampers is below 8 Volt, therefore the supplied voltages V_1, V_2 or V_3 can be easily modulated to the desired level using regular electrical resistances R_1, R_2 and R_3. In the case of tuning the voltages to a different level, these resistances can be easily replaced; adjustable resistances can also be used for tuning purposes.

Once the electrical plate and its peripheral circuits have been manufactured, the next step is to sample the voltage from the plate for commanding the MR damper. In a conventional way, such displacement feedback is achieved by sensor detection. For example, linear variable differential transducers (LVDT) or string pots can be used to detect the magnitude of the damper piston movement, and then the detected signal will be received by the microcontroller for calculating the output voltage. However, for the proposed control logic, the required input is simply the damper piston movement. Thus, a sampling pin can be rigidly attached to the damper piston which will swipe over the electrical plate with the movement of the piston. If the center of the electrical plate can be adjusted to align with the zero position of the piston, the displacement and control voltage relationship can be made to agree with the governing equation of the SPSAC logic in Eq. (7).

A rendering of hardware emulation of the SPSA Crule is illustrated in Fig. 10. The mechatronics device consists of two main parts: a sampling pin and an electrical plate. The pin is attached to the damper piston and the electrical plate is attached to the damper casing or to the fixture to which the damper is tied down. The pin is able to sample the voltage from the electrical plate depending on the piston displacement and input this voltage to the MR damper. The voltage distribution on the electrical plate is designed based on control logic in Eq. (7). It is observed from Fig. 8 that a voltage V_1, V_2, or V_3 may still be input to the damper after the motion stops, depending on the final displacement of the piston (permanent deformation in case of nonlinear structural behavior). In the hardware implementation of the control logic in Fig. 10, a motion detector switch can be installed in the damper to automatically shut down the power when MR damper piston stops moving or if the motion is below certain threshold.

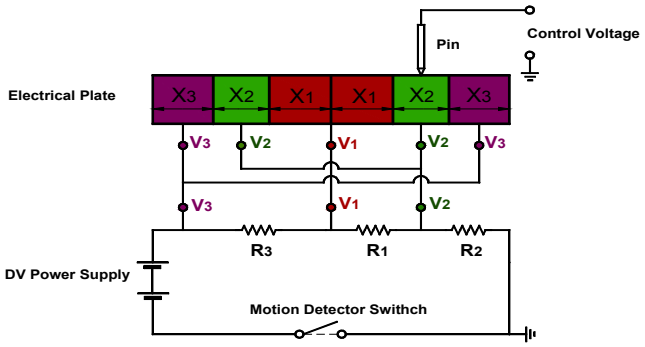

Fig. 9 Hardware Emulation of the Proposed SPSAC Algorithm

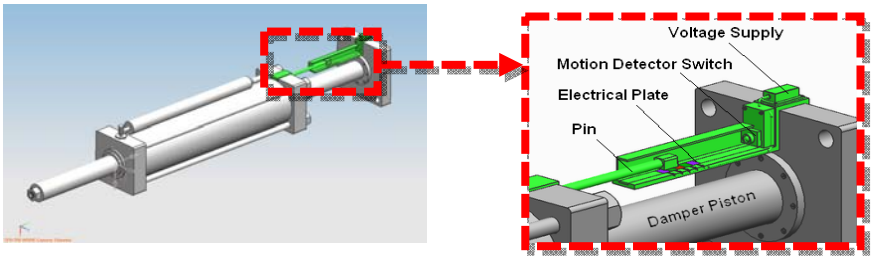

Fig. 10 Rendering of Hardware Emulation of the Proposed SPSAC Algorithm

A typical MR damper semi-active control system requires sensors and controller shown by shaded region in Fig. 11 below. Performance of the control system may be affected by undesired interference between the MR damper and these components. For example, electromagnetic interference to the adjacent circuits and devices may occur due to the presence of the massive wired coil embedded inside of the MR damper piston.

The typical MR damper control system can be simplified to the system shown in the green dashed block in Fig. 11 because of the elimination of sensors and controllers as separate components in the SPSAC mechanism. Hence, the proposed SPSAC mechanism is more reliable than a typical control system.

6. Performance of the simple passive semi-active controller

A three-story structure has been used to carry out detailed investigation on performance of the SPSAC algorithm. This building represents 60% scaled down frame of a building designed for stiff soil location in Los Angeles, CA, and was used for carrying out large scale testing of MR dampers (Jiang *et al*. 2010). Fig. 12 shows the evaluation model of the building. The first three modal frequencies of the reduced model are 1.13 Hz, 3.69 Hz, and 8.44 Hz. It is noted that only the DOFs in the horizontal direction are considered in the reduced model.

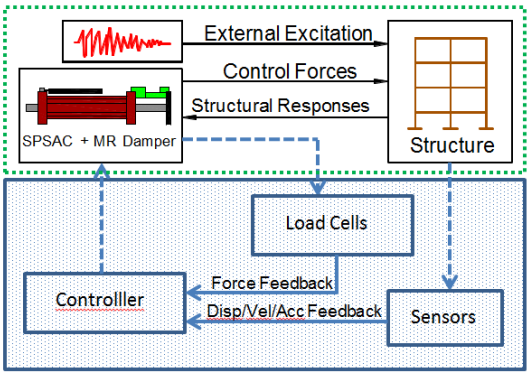

Fig. 11 Comparison between MR Damper Control Systems: (a) Conventional, (b) SPSAC Mechanism

Four DOFs are associated with the corresponding floors, while remaining DOFs No. 5, 6, and 7 are located at the Chevron braces joints. In this evaluation model, one 200 kN MR damper is assumed to be horizontally installed on each of the three above-ground floors, as shown in Figure 12. The positive control force generated by the MR dampers is applied at the Chevron brace joints (DOFs 5, 6, 7) and the negative damper forces are applied on the floors (DOFs 1, 2, 3). Bouc-Wen model has been used to model MR dampers in numerical simulations. Detailed information on the model in Fig. 12 can be found in Zhang (2012).

In addition to ground motions described previously, additional 60 recorded ground motions from the SAC project ground motion suites have been selected. These 60 ground motion records, which were used for the analysis of buildings located in Los Angeles, include records from historic earthquakes as well as artificially-generated time histories based on the modeling of the rupture process and wave propagation through the soil strata. Among these 60 ground motion records, 22 ground motions have peak accelerations smaller than 0.4 g, 20 ground motions have maximum accelerations varying between 0.4 g and 0.7 g and remaining 18 ground motions have peak accelerations larger than 0.7 g. Hence, numerical simulations have been carried out using 64 earthquakes. Performance of MR dampers with the proposed SPSAC has been compared with the performances of MR dampers with clipped-optimal controller (COC), smooth-boundary-layer controller (SBLC), and the passive-on (PON) controller. Parameters for designing these controllers are: $q = 5 \times 10^6$, $r = 1$ for COC, $\alpha = 1000$, $\beta = 120$ for SBLC and X_1=0.008, X_2=0.004, X_3 = 0.001, V_1=7.5V, V_2=0Vand V_3 = 7.5V for the SPSAC. The saturation voltage for all controllers is V_{max} = 7.5 V.

It has been observed from simulation results that the performance of SPSAC is the best among all controllers, including PON, during all 4 previously described earthquakes, although other controllers also have a performance similar to SPSAC during some earthquakes. For example, interstory drifts using different controllers during the Northridge earthquake show that the performances of SPSAC, PON and SBL controllers are quite close to each other and are significantly better than that of the COC.

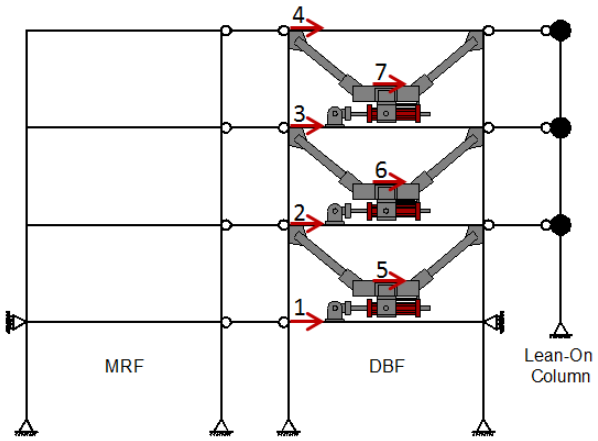

Fig. 12 Evaluation model of a 60% Scaled-Down Frame of a Prototype Building

Because of space limitations, only evaluation criteria J_1 andJ_2 in Table 1 have been calculated for MR dampers with all control strategies (PON, COC, SBLC, SPSAC, and SPB) under all 64 earthquakes. Since the objective is to compare performance of SPSAC with respect to other control strategies, we define "Gain/Loss Ratio of J" ($GLRJ$) for comparison as

$$GLRJ_{Control\ B,i}^{Control\ A,EQ} = \left[\left(J_i^{Control\ B,EQ} - J_i^{Control\ A,EQ}\right)/J_i^{Control\ B,EQ}\right] \times 100\% \quad (8)$$

In Eq. (8), $GLRJ_{Control\ B,i}^{Control\ A,EQ}$ calculates "the Gain/Loss ratio of control strategy A over control strategy B in terms of evaluation criteria J_i under earthquake EQ". We use $GLRJ$ instead of GLJ defined in Eq. (5), since $GLRJ$ is a more reasonable and fair evaluation quantity for large number of control scenarios. For instance, we consider performance of control strategies A and B during EQ1 and EQ2 as: (1) $J_i^{Control\ B,EQ1} = 0.2$, $J_i^{ControlA,EQ1} = 0.1$; (2) $J_i^{ControlB,EQ2} = 0.9$, $J_i^{ControlA,EQ2} = 0.8$. Then, based on the definition of GLJ in Eq. (5), $GLJ_{ControlB,i}^{ControlA,EQ1}$ and $GLJ_{ControlB,i}^{ControlA,EQ2}$ are both calculated as 10%. However, the reduction from 0.2 to 0.1 in the first case is more significant than the reduction from 0.9 to 0.8 in the second case, because the first case has a reduction of 50% whereas the second case has a reduction of mere 11.1%. During a moderate earthquake, some of the evaluation criteria can be smaller than 0.1. However, during a severe earthquake, these criteria can increase to more than 0.8, since the evaluation criteria in Table 1 are normalized using the maximum of peak uncontrolled response quantities for a particular earthquake. The performance measure $GLRJ$ addresses this issue.

Since the purpose of this study is to investigate the performance of the SPSAC, $GLRJ$ values have been calculated for SPSAC with respect to COC, SBLC, and PON cases for evaluation criteria J_2 (interstory drift) for all 64 earthquakes. Other criteria have not been presented because of space limitations. Figs. 13 shows plots of $GLRJ$ values for SPSAC with respect to COC, SBLC, and PON cases for J_2.

It is observed from Fig. 13 that all values of GLRJ for SPSAC with respect to COC are positive, implying that the SPSAC always performs better than COC in reducing the interstory drift. When compared with SBLC, there are only two negative $GLRJ$ values. In these cases also, performance of SPSAC is almost similar to SBLC. For SPSAC with respect to PON, there is only one negative value of GLRJ, which is close to zero. Hence, performance of SPSAC is generally better than those of COC, SDLC and PON.

Based on extensive simulation results, Table 2 shows average values of $GLRJ$ for SPSAC with respect to COC, SBLC, and PON cases for evaluation criteriaJ_1, J_2 and J_3. It is observed that the SPSAC case has a significantly superior performance over other two semi-active controllers (COC and SBLC) in reducing peak displacement, peak inter-story drift, and cumulative floor drift. However, it has only slightly better average performance than the PON case in reducing all three response quantities.

Table 2 Average GLRJ: SPSAC vs COC, SBLC, and PON

$GLRJ_{COC,1}^{SPC,Average}$	+72.95%	$GLRJ_{SBLC,1}^{SPC,Average}$	+43.65%	$GLRJ_{PON,1}^{SPC,Average}$	+4.41%
$GLRJ_{COC,2}^{SPC,Average}$	+69.54%	$GLRJ_{SBLC,2}^{SPC,Average}$	+36.63%	$GLRJ_{PON,2}^{SPC,Average}$	+4.21%
$GLRJ_{COC,6}^{SPC,Average}$	+71.65%	$GLRJ_{SBLC,6}^{SPC,Average}$	+40.70%	$GLRJ_{PON,6}^{SPC,Average}$	+3.63%

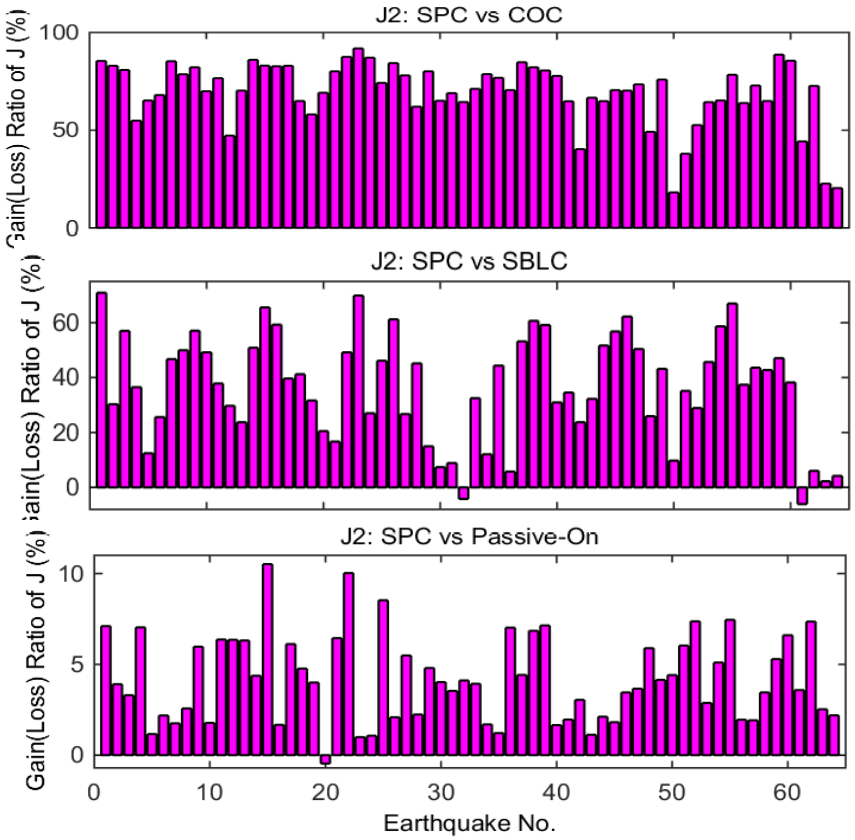

Fig. 13 Plots of Gain/Loss Ratio of J between SPC and COC, SPC and SBLC and SPC and PON

7. Conclusions

This paper presents an investigation on the performance of large-scale MR dampers controlled by semi-active and passive algorithms. Simulations models of MR dampers are based on testing data on 200 kN large scale MR dampers. It is observed that the energy dissipations of semi-active controllers are almost similar or even inferior to those of PON cases. Based on energy dissipation pattern by MR dampers in semi-active and PON modes, an innovative controller, termed as simple passive semi-active controller, is proposed for the control of MR dampers. The controller maximizes energy dissipation and can be emulated by hardware, thereby eliminating the need for sensors and controllers. It is observed that the SPSAC performs better than other semi-active controllers and the PON cases. Performance of the SPSAC algorithm has been verified through extensive numerical time-history analysis. It is mentioned that the performance of the SPSAC has also been verified through large scale real-time hybrid testing. The hardware emulation of the SPSAC has also been tested in the laboratory. Results on these tests will be presented in future publications.

Acknowledgements

This research is supported by the grant from the National Science Foundation (NSF) NEESR Grant No. CMMI-1011534. Any opinions, findings, and conclusions expressed in this paper are those of the authors and do not necessarily reflect the views of the sponsors.

References

Agrawal, A., Tan, P., Nagarajaiah, S. and Zhang, J. (2009), "Benchmark structural control problem for a seismically excited highway bridge—Part I: Phase I problem definition", *Struct. Control Health Monit.*, **16**(5), 509-529.

Bass, B.J. and Christenson, R.E. (2007), "System identification of a 200 kN magneto-rheological fluid damper for structural control in large-scale smart structures", *Proceedings of the 2007 American Control Conf.*, July 11-13, 2007, New York, NY.

Carlson, J.D. and Spencer Jr., B.F. (1996), "Magneto-rheological fluid dampers for semi-active seismic control", *Proceedings of the 3rd Int. Conf. on Motion and Vibr. Control* , Chiba, Japan.

Carlson, J.D., Catanzarite, D.M. and St. Clair, K.A. (1996), "Commercial magneto-rheological fluid devices", *I. J. Modern Physics B*, **10**, 2857-2865.

Chen, Z.Q., Wang, X.Y., Ko, J.M., Ni, Y.Q., Spencer Jr., B.F. and Yang, G. (2003), "MR damping system on Dongting Lake cable-stayed bridge", *In Smart Structures and Materials, International Society for Optics and Photonics*, 229-235.

Chopra, A.K. (2001), *Dynamics of Structures: Theory and Applications to Earthquake Engineering*, Prentice Hall, New Jersey.

Friedman, A., Dyke, S., Phillips, B., Ahn, R., Dong, B., Chae, Y., Castaneda, N., Jiang, Z., Zhang, J., Cha, Y., Ozdagli, A., Spencer, B., Ricles, J., Christenson, R., Agrawal, A. and Sause, R. (2014), "Large-scale real-time hybrid simulation for evaluation of advanced damping system performance", *J. Struct. Eng. - ASCE* ,10.1061/(ASCE)ST.1943-541X.0001093 , 04014150

He, W.L., Agrawal, A.K. and Yang, J.N. (2003), "Novel semiactive friction controller for linear structures against earthquakes", *J. Struct. Eng.- ASCE* , **129**(7), 941-950.

Jansen, L.M. and Dyke, S.J. (2000), "Semiactive control strategies for MR dampers: comparative study", *J. Eng. Mech. - ASCE*, **126**(8), 795-803.

Jiang, Z., Mantoni, D., Christenson, R., Chae, Y., Ricles, J., Friedman, A., Dyke, S., Phillips, B. and Spencer Jr., B.F. (2010), "Comparison of 200 KN MR damper models for use in real-time hybrid simulation", *Proceedings of the 5th World Conference on Structural Control and Monitoring,* 12-14 July 2010, Tokyo, Japan, Paper No. 5WCSCM- 10325.

Spencer Jr., B.F. and Nagarajaiah, S. (2003)"State of the art of structural control", *J. Struct. Eng. - ASCE*, **129**(7), 845-856.

Spencer Jr., B.F., Dyke, S.J., Sain, M.K. and Carlson, J. (1997), "Phenomenological model for magnetorheological dampers", *J. Eng. Mech. - ASCE*, **123**(3), 230-238.

Spencer Jr., B.F., Yang, G., Carlson, J.D. and Sain, M.K. (1998a), "Smart dampers for seismic protection of structures: a full-scale study", *Proceedings of the 2nd World Conf. Struct. Control*, Kyoto, Japan.

Ohtori, Y., Christenson, R., Spencer Jr., B.F. and Dyke, S. (2004), "Benchmark control problems for seismically excited nonlinear buildings", *J. Eng. Mech. - ASCE* , **130**, 366-385.

Taylor Devices (2012), "Structural applications of fluid viscous dampers", http://www.taylordevices.com/pdf/2011-StructuralApp.pdf.